Buitrago, M.; Bertolesi, E.; Juan Sagaseta; Calderón García, PA.; Adam, JM. (2021). Robustness of RC building structures with infill masonry walls: tests on a purpose-built structure. Engineering Structures. 226:1-15. https://doi.org/10.1016/j.engstruct.2020.111384

Robustness of RC building structures with infill masonry walls: tests on a purpose-built structure

Manuel Buitrago[a], Elisa Bertolesi[a], Juan Sagaseta[b], Pedro A. Calderón[a], José M. Adam[a]*

[a]ICITECH, Universitat Politècnica de València. Camino de Vera s/n, 46022 Valencia, Spain
[b]Department of Civil and Environmental Engineering, University of Surrey, GU2 7XH Guildford, UK

* Corresponding author. Tel.: +34 963877562; fax: +34 963877568.
E-mail address: joadmar@upv.es (José M. Adam).

Abstract

Structural robustness is a significant property towards improving resilience of buildings, i.e. enhance their ability to withstand and recover from extreme events which often can cause local damage and progressive collapse. It is widely accepted that robustness depends on the capacity of the structure to activate alternative load paths (ALPs) after the failure of load-bearing elements, e.g. columns. Early evidence during World War II showed that progressive collapse of some buildings was avoided by the presence of masonry infill walls. Subsequent studies focused on this effect for cases of sudden column removal although most of these studies were analytical, numerical and only looked at internal columns which are generally less vulnerable to accidental events compared to corner and edge columns. The aim of this study was to analyse how infill walls can improve the robustness of reinforced concrete (RC) buildings in corner columns failure scenarios. A purpose-built 3D two-storey full-scale RC building structure with infill masonry walls was tested. The contribution of masonry infill walls was analysed in terms of: i) load redistribution, ii) ALPs, and iii) Dynamic Amplification Factors (DAFs) to be applied in linear-static analyses. The test was highly monitored by 38 strain gauges, 38 LVDTs and 2 accelerometers to register the vertical and lateral response. The results showed that masonry infill walls had a significant influence on the structural response and activated the predominant ALPs at very small deflections.

Keywords: *Extreme events, Infill masonry walls, Progressive collapse, RC structures, Corner-columns, Building, Robustness.*

1. Introduction

Enhancing the resilience of our society against natural and man-made disasters is a challenge included in the main agenda of many international research programmes such as European Horizon 2020. In order to design and construct resilient buildings and infrastructure (able to withstand and recover from extreme events) structural robustness needs to be considered to limit the extent of damage or even progressive collapse [1] after local failure of some of it structural members. Building codes such as DoD [2], GSA [3] and EC [4] adopt different methods for robustness design including the Alternative Load Path (ALP) method in which a minimum level of robustness is verified using the notional column removal concept.

Many studies have been carried out applying column removal to buildings [5] to determine the ALPs that the structure can activate after local failure. The most important ALPs identified in the literature [5,6] are: i) flexural action in the slabs, ii) the Vierendeel beam effect of the frame, iii) compressive and tensile membrane action, and iv) the contribution of infill walls (i.e. secondary trusses). Regarding the ALP provided by infill walls, pioneering work by Baker et al. [7] in 1948 and Christopherson [8] in 1945 based on forensic investigations of damaged buildings after World War II showed clear evidence where progressive collapse was prevented by infill panelling. Subsequent research in this area focused on column removal scenarios [9–21] and internal column removal in particular. Corner columns are more vulnerable to extreme events (e.g. vehicle impacts, blast) compared to internal columns and therefore this is a relevant subject. For corner column removal, the only work available investigating the role of infill panels is analytical and numerical (e.g. Hafez et al. [14], Farazman et al. [15], Helmy et al. [16] and Xavier et al. [17]) or experimental with 2D and single frame-walls (e.g. Baghi et al. [22] and Brodsky et al. [23,24]). Therefore there is a gap of experimental evidence which is addressed in this paper.

The activation of some ALPs in corner column removal cases can be challenging. For example, compressive membrane action cannot be activated due to the lack of in-plane restraint at the edges of the bay of the removed column. Tensile membrane action is also less effective in corner-column scenarios [25] and therefore the presence of infill walls can be critical for activating sufficient ALPs to arrest the propagation of failure [14–17]. There are also questions on whether vertical ties in the columns are needed to activate the infill ALP and how dynamic effects might influence the response.

The aim of this work was to study the contribution of infill masonry walls in corner-column removal scenarios by means of a purpose-built 3D full-scale RC building structure. To the authors' best knowledge this test is the first of this kind and it allows a direct comparison with the results from the case without infill walls presented in Adam et al. [26]. Another novelty of this work was the use of realistic gravity loads used in design for accidental loading. A further aim was to obtain Load Increase Factors (LIFs) and Dynamic Amplification Factors (DAFs) that could assist engineers and architects in designing building structures with infill walls by means of simplified linear static analyses.

After the Introduction, the paper is structured as follows: Section 2 describes the building investigated, Section 3 describes the test carried out together with the monitoring system used, Section 4 presents the time-history results in terms of vertical and horizontal displacements and acceleration of the structure, displacements of the infill walls, strains on columns and the residual damage in the structure. Section 5 analyses and discusses the influence of infill masonry walls on load redistribution, ALPs and LIFs/DAFs, while the main conclusions are given in Section 6.

2. Description of the specimen building

The study was carried out on a full-scale purpose-built structure that had been used in previous studies [26] to assess its structural dynamic performance without infill walls in corner-column failure scenarios. The dimensions included: span lengths of 5m, 300x300mm^2 columns, 200mm thick flat-slabs, nominal cover of columns and slabs was 30mm, and floor-to-ceiling heights of 2.8m (see Fig. 1). Reinforcement ratios for slabs were similar for the 1st and the 2nd floor (around 0.6% at mid-span and 1% near the edge columns) whereas for the column members the reinforcement ratio was between 0.9% and 1.4%. Further details can be found in Adam et al [26]. In addition, the present study included infill masonry walls in the first-floor façade frame from

P1-P7 and P7-P9, as shown in Fig. 1, as a main difference with the previous referenced study. Bricks measuring 245x113x90mm were laid in a stretcher/running bond arrangement to form a solid wall.

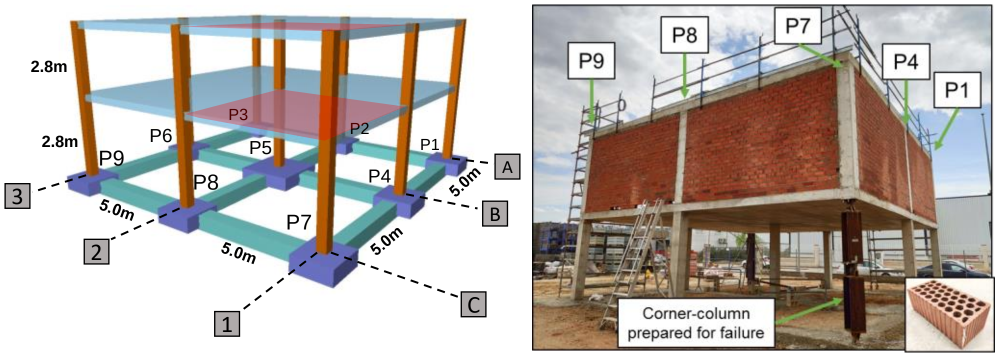

Fig. 1. Sketch and view of the building structure with infill masonry walls.

The test took place 69 days after placing the concrete of the second floor slab and 21 days after building the infill masonry walls. The mechanical properties of the materials of the different elements were determined at different curing ages. The tensile strength of the concrete was only obtained for slabs; mean values obtained at the day of the test are shown in Table 1.

Table 1. Mechanical properties of concrete (columns and slabs), mortar and bricks (infill walls).

Mechanical property	Element	Age [days]	Results [MPa]
Compressive Strength *4 concrete cylinders per element; 300x150mm (EN 12390-3)*	Ground floor columns	92	35.9
	1st slab	78	34.2
	1st floor columns	77	33.6
	2nd slab	69	32.6
Elastic Modulus *3 concrete cylinders per element; 300x150mm (EN 12390-13)*	Ground floor columns	92	32229
	1st slab	78	30849
	1st floor columns	77	28972
	2nd slab	69	32479
Tensile Strength *3 concrete cylinders per element; 300x150mm (EN 12390-6)*	1st slab	78	2.31
	2nd slab	69	2.62
Flexural Strength *3 concrete prisms per element; 600x150x150mm (EN 12390-5)*	1st slab	78	4.76
	2nd slab	69	4.10
Mortar Compressive Strength *3 cubes; 40mm (EN 1015-11)*	Infill masonry walls	21	14.4
Bricks Compressive Strength *3 bricks (EN 772-1)*	Infill masonry walls	---	16.0

3. Test and monitoring

3.1. Description of the corner-column failure scenario

The failure scenario studied consisted of the sudden removal of a corner column (P7) on the ground floor in the opposite corner to the one (P3) used for a previous test (Test 1; Adam et al. [26]) to avoid any possible structural defects influencing the results. The test was performed using gravity loads obtained from accidental load combinations used in design [2–4,27]. The GSA guidelines were followed [3] with 1.2DL+0.5LL, which resulted in an additional nominal load of 4.9kN/m^2 [5kN/m^2 (self-weight), 2kN/m^2 (dead loads), 3kN/m^2 (live loads)]. This load was applied to each floor in the bay nearest to the P7 corner column (see Fig. 2) using uniformly distributed concrete blocks. The final load arrangement of the concrete blocks resulted in a uniformly distributed load of 5.3kN/m^2 applied on the corner bay at the first and second floor (See Figs. 1-2).

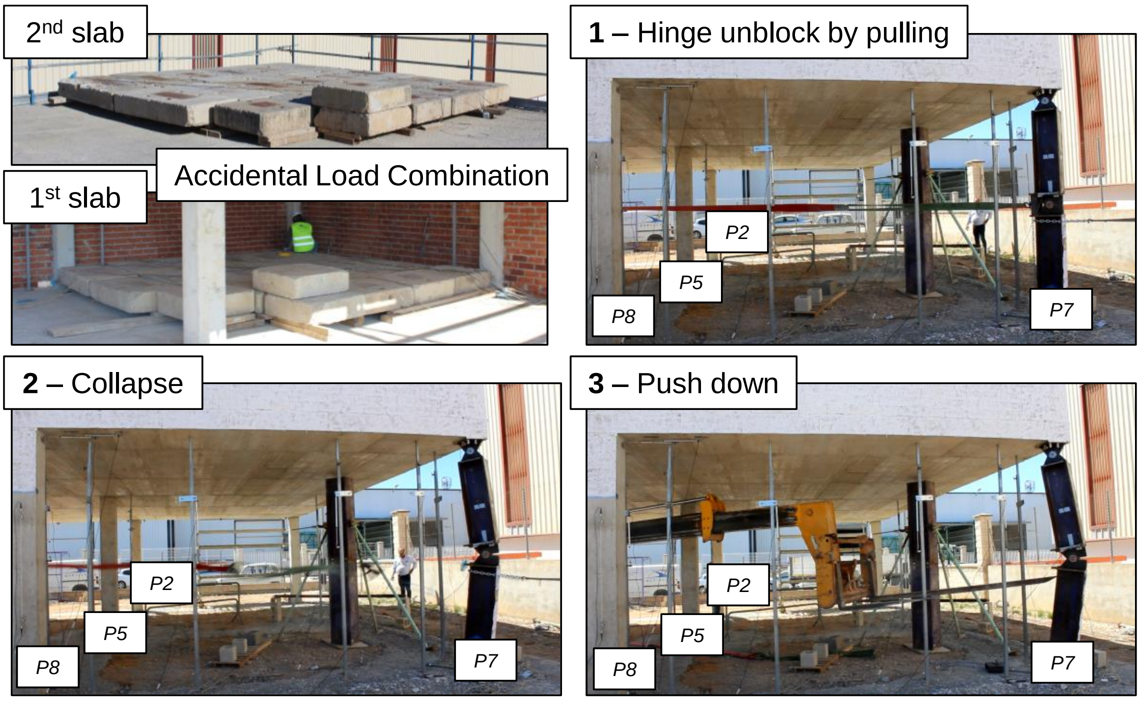

Fig. 2. Loads on slabs for the accidental load combination and reproduction of the failure scenario including the last push down step.

A specially designed steel column was used for the sudden removal of corner P7 which had three hinges, a central and one at each end, that were activated during the test. The central hinge remained locked by different safety components until the start of the test, when they were unlocked for activation. The system had been used in previous tests (Test 1) by the present authors and further details can be found in [26].

Test 2 presented in this paper was divided into two steps: i) the first step (referred as "column removal step") corresponded to the sudden removal of the corner column, and ii) a subsequent step with pushing of the removed corner-column P7 (referred as "push down step") which resulted in a push-down force. The push down step was carried out gradually (quasi-static) to evaluate the evolution of the ALPs in the structure for larger deformations (see Section 4.4 for more information); the maximum down force applied was of similar value to the axial load in column P7 before it was removed. The push down step took place one hour after the column removal step. Fig. 2 shows the different test phases from the unlocking of the central hinge and column removal to the final push down step. An extra steel column can also be seen in Fig. 2, which was not connected to the structure and it was placed below the first slab only for safety reasons during the test.

3.2. Monitoring

The monitoring system contained a high frequency data acquisition device (200 samples per second) plus different types of sensors: LVDTs for displacements (38 units), strain gauges (38 units) and fibre optic accelerometers (2 units). Figs. 3 and 4 show the LVDTs used to measure vertical displacements on slabs and columns P4 and P8 near the foundation at the side nearer P7; the figures also show the LVDTs used to measure horizontal displacements to monitor the total drift of the structure. All the LVDTs were labelled following the pattern LVDT-Column-XYZ, where X indicates the floor (1 or 2 depending on the first or second slab), Y indicates the number and position of the LVDTs, and Z adopts letters H or V which means horizontal or vertical, respectively. The positions of the accelerometers are also given in Fig. 3a which were placed on column P7-first floor in the vertical direction and on column P1-second floor in the horizontal direction. Fig. 3b (b1 and b2) shows the location of four strain gauges installed on the reinforcement bars of each first-floor (P1, P4, P5 and P8) and second-floor column (P4, P5, P7 and P8), while three were fitted to the web and flange of the HE-300B profile in the steel columns P3 and P7. These were labelled following the pattern SG_Column-XY, where X indicates the columns floor (from 0 to 1 for the ground and first columns floor) and Y indicates the number and position of the strain gauge (from 1 to 4). One of the infill masonry walls was monitored (between columns P7 and P8), as shown in Fig. 3c, with three LVDTs to measure transverse strain (tension) to the compressive diagonal, placed from column P7 on the second floor slab to P8 on the first floor slab (MT-top, MM-middle and MB-bottom), and two LVDTs to measure the masonry detachment from the concrete structure (MDV-masonry detachment in vertical direction and MDH-masonry detachment in horizontal direction).

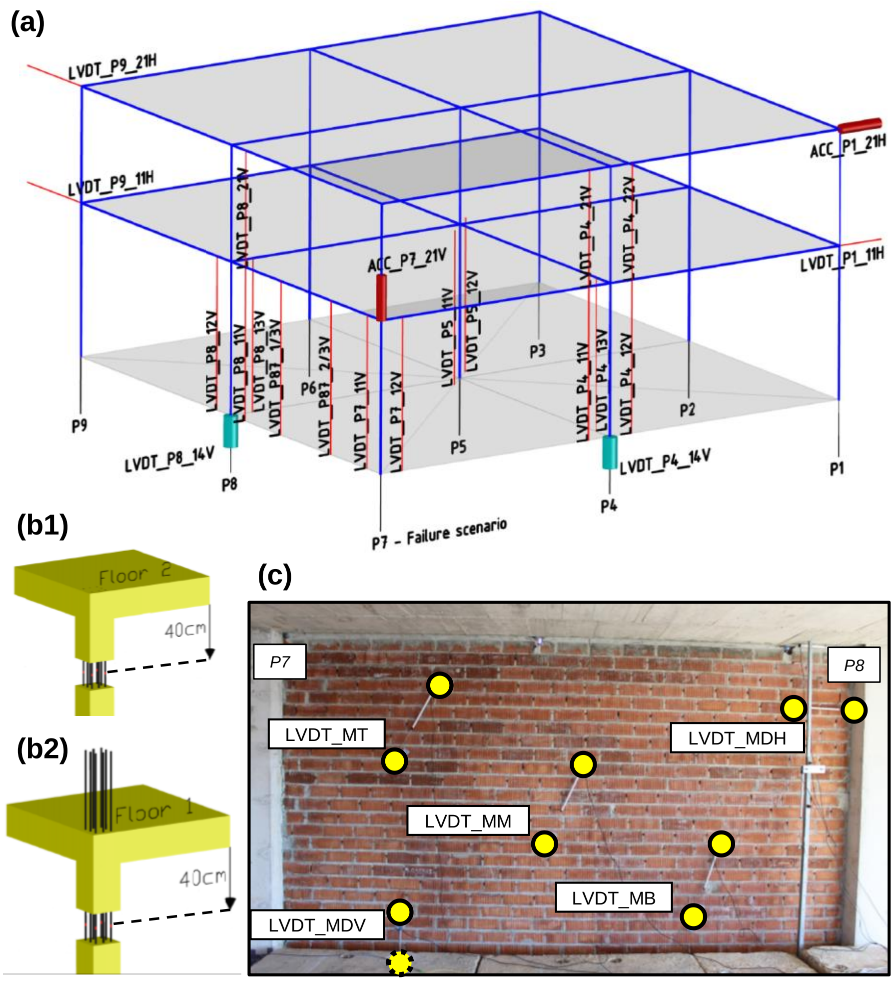

Fig. 3. Position of accelerometers and LVDTs for vertical displacements and drift values (a), strain gauges on ground (b2) and 1st (b1) floor columns, and LVDTs in the internal face of the infill masonry wall between columns P7 and P8 (c).

Horizontal LVDTs, used to measure bending of the slab-column joint, were placed on the top and bottom slab surface connected to both slabs and columns. Fig. 4 shows the positions of the sensors on the first and second floor and some pictures as an example of the installation of these sensors on the bottom of slabs. Most of the instrumentation used in Test 2 was placed in similar positions as Test 1 (Adam et al [26]) for comparison of test results.

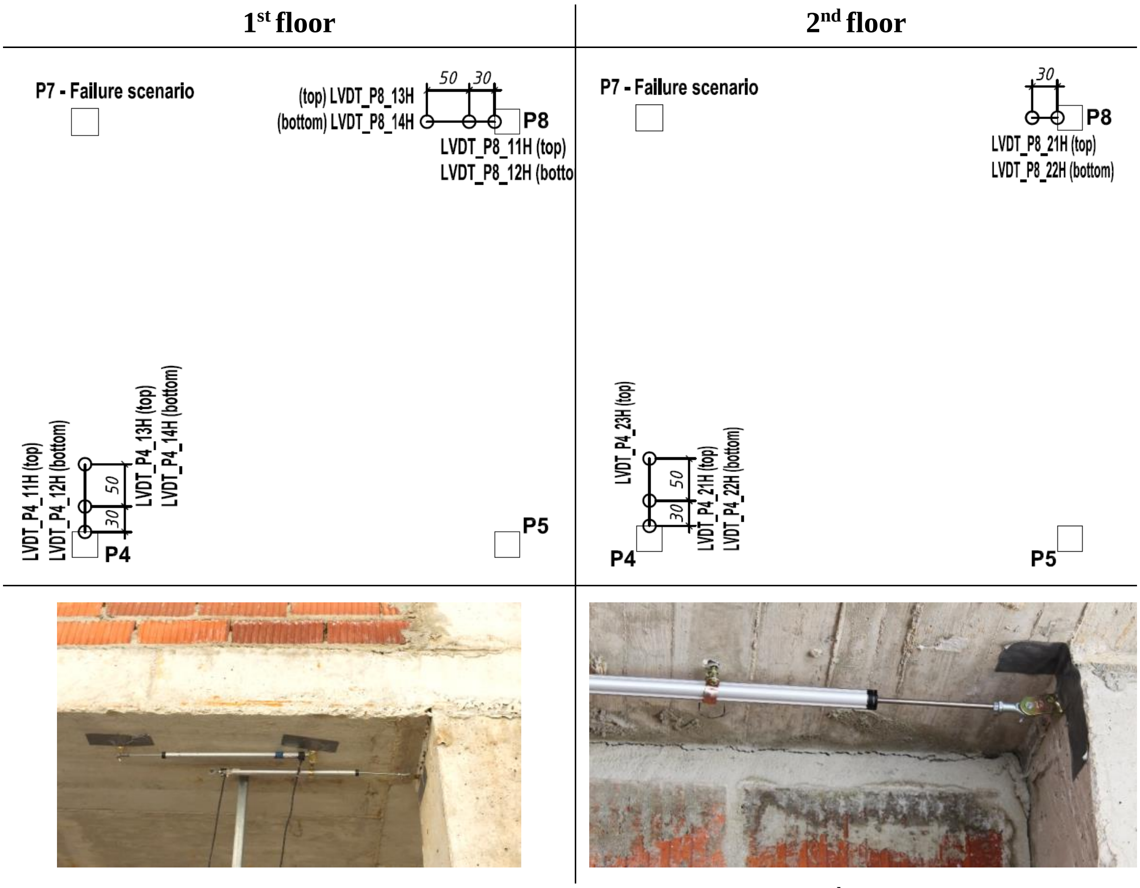

Fig. 4. Position of horizontal LVDTs on the 1st and 2nd floor.

4. Time-history results

4.1. Vertical displacements

Fig. 5 shows the maximum vertical displacement recorded by one of two LVDTs placed close to the removed column between *t*=0s and *t*=10s. Both sensors (P7_11V and P7_12V) recorded almost identical readings, with a maximum vertical displacement of 7.8mm and a damped vibrational behaviour after the sudden removal. The maximum vertical displacement was 17.3mm in the subsequent push down step (between *t*=10s and *t*=22s) which was significantly larger than the one measured after the sudden column removal as shown in Fig. 5.

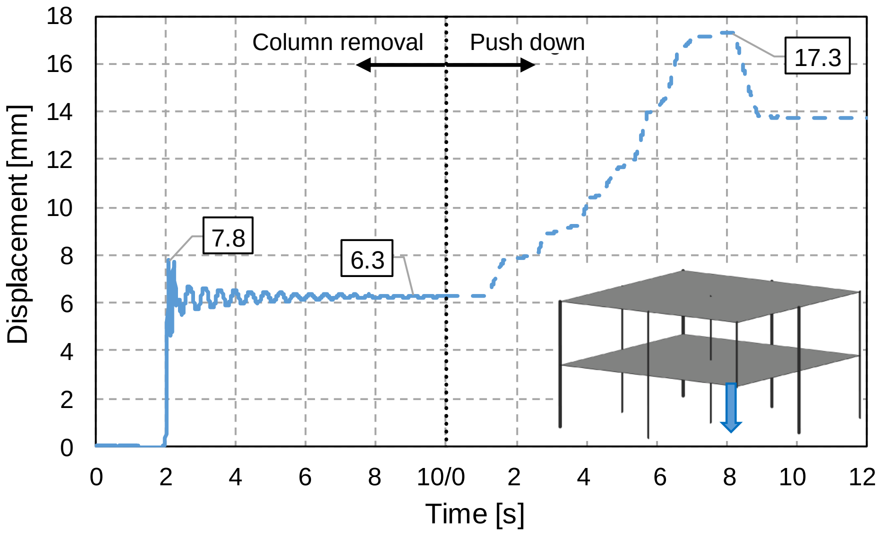

Fig. 5. Vertical displacement of the 1st floor in column P7 during the test.

Four LVDTs (P8_11V, P87_1/3V, P87_2/3V and P7_11V) were used to monitor the vertical deformation profile along of the first slab between columns P7 and P8 (see Fig. 3a). Fig. 6 shows the results obtained in the test, together with sensor positions and the maximum and residual displacements obtained. In the column removal step the peak/residual displacement value ratios ranged from 1.26 (P7_11V) to 1.35 (P87_1/3V). These results are representative of the dynamic amplification of the displacements which are analysed in further detail in Section 5.3.2.

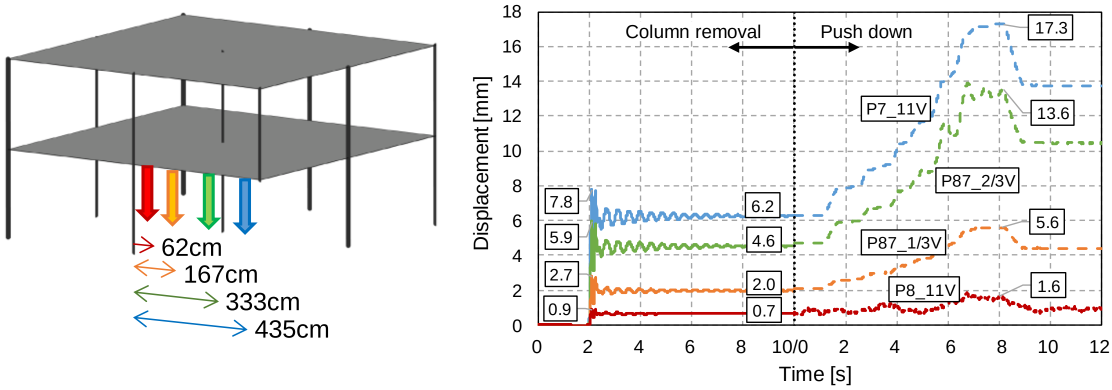

Fig. 6. Vertical displacements of the 1st slab between columns P8 and P7 during the test.

4.2. Horizontal displacements

Horizontal LVDTs were placed on the structure to measure: a) bending of the slab-column joints adjacent to the removed column (assessment of flexural and Vierendeel effects); and b) drift of the structure due to the global eccentricity of the loading. Fig. 7 shows the time-history results of the horizontal displacement sensors (11H, 12H, 21H and 22H) on the columns nearest to the removed column (P4 and P8) on the first and second floors (see sensors positions in Fig. 4). The horizontal deflections obtained were small and, in general, shortening (compression) relative displacements (12H and 22H) were higher than elongation (tension) relative displacements (11H and 21H). These results suggested that cracking of the slabs was insignificant as visually confirmed during the test.

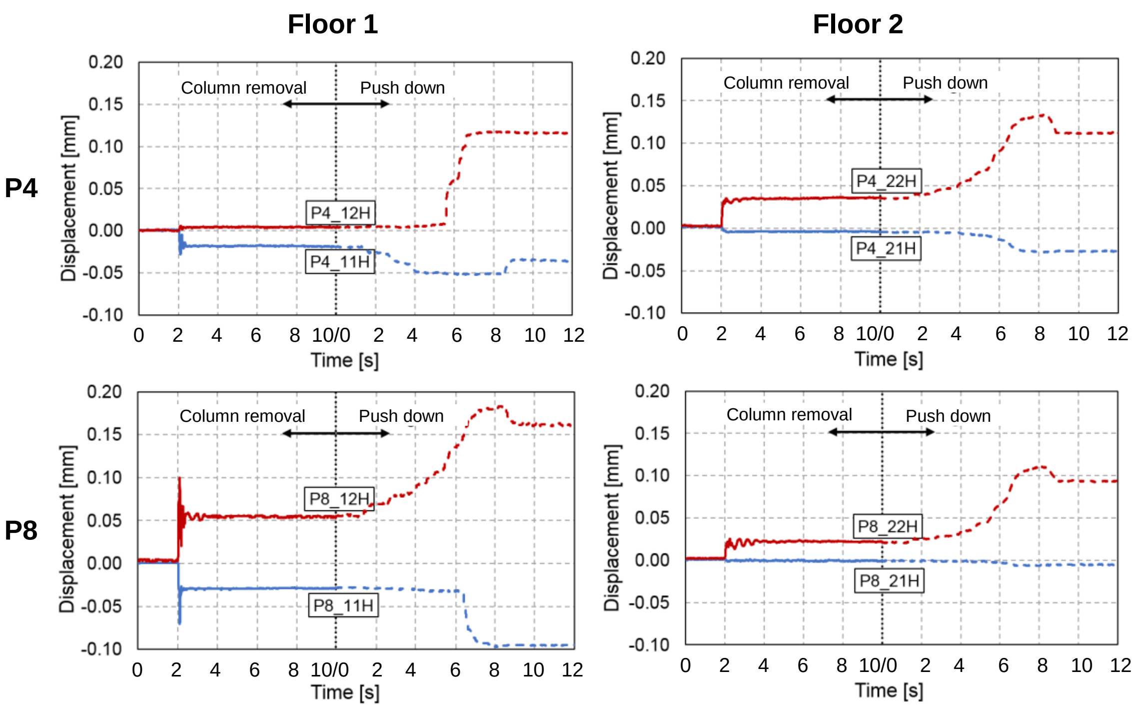

Fig. 7. Horizontal relative displacements on slabs near columns P4 and P8 on the first and second floors. Positive values represent shortening (compression) relative displacements.

Fig. 8 shows the time-history results for the drift of the structure during the test. Sensor positions are shown in Fig. 8 (see also Fig. 3). Maximum horizontal displacements on the first floor measured at columns P1 and P9 in both orthogonal directions were lower than 2mm. The results on the first floor also show the negligible residual horizontal movement of the structure compared to the peak values obtained during the vibration. The displacement peak and residual value ratio on this floor ranged from 2.7 (P9_11H) to 3.8 (P1_11H). Horizontal displacement of the structure was also negligible during the push down step.

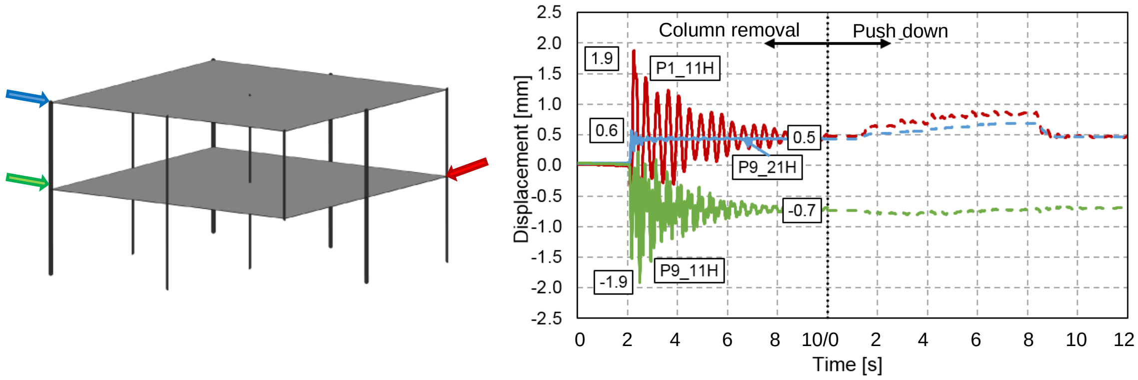

Fig. 8. Drift of the structure during the test. Positive values follow the direction of the arrows.

4.3. Displacements on the infill masonry wall

The LVDTs placed along the compressive diagonal (MT, MM and MB in Fig. 3c) did not register significant displacements in the test. This suggests that the tensile strains within the infill masonry walls were low because they were not fully connected with the concrete frame. This also meant that cracking in the wall was insignificant, as observed in the test (see Section 4.6).

The LVDTs measuring the degree of masonry detachment from the concrete frame captured significant displacements, which confirmed that the mortar failed at the concrete-masonry interface (see Section 4.6 for further details). Fig. 9 shows the time-history results from the LVDTs MDH and MDV (see Fig. 3c) which measured the concrete/masonry detachment at the top of column P8 in the horizontal direction and at the bottom of the wall in the vertical direction respectively. During the column removal step, the horizontal and vertical detachment was 1.2mm and zero respectively whereas during the push down step, the maximum horizontal and vertical detachment was 5.6mm and 0.9mm respectively. This shows that the structure separated from the infill walls, especially during the push down step, at the corners of the wall near the second floor column P8 and first floor column P7.

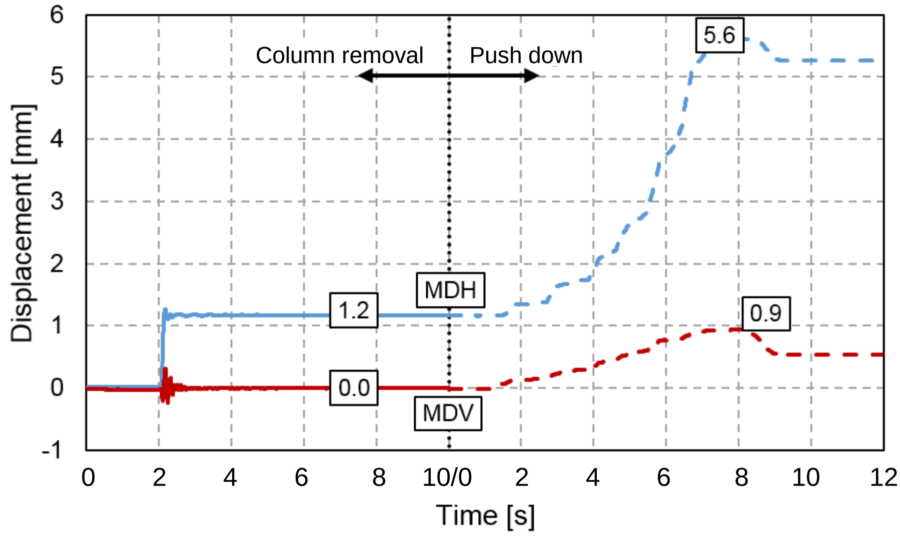

Fig. 9. Masonry detachment from the concrete structure during the test.

4.4. Strain on columns

Fig. 10 shows the mean elongation of the removed column (P7_0) obtained from three strain gauges on the steel column. From these measurements it was estimated the load on the column before removal (48με – 150kN) as well as the removal time (0.07s) and the pulling load during the push down step (38.6με – 121kN; as a result of 86.6με - 48.0με).

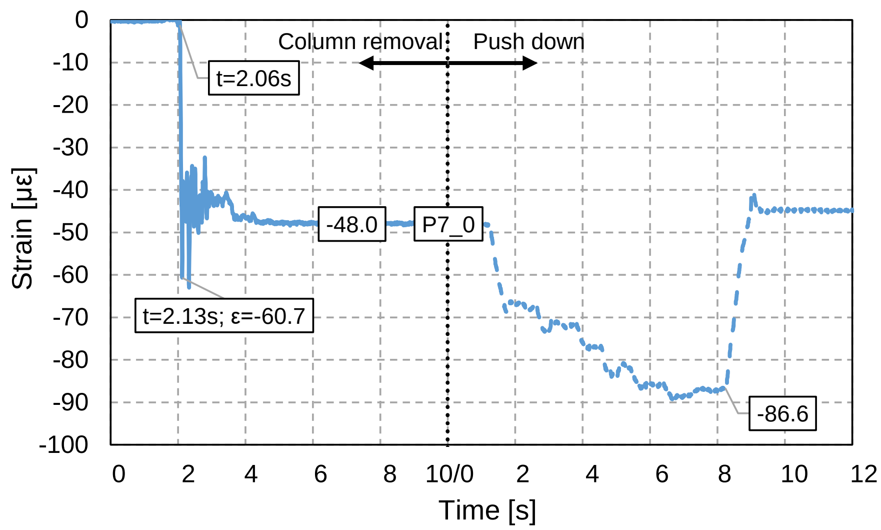

Fig. 10. Mean value of strain gauges on the ground floor column P7 (negative values indicate elongation (decompression)).

Columns P4, P5 and P8 adjacent to P7 were also monitored using four strain gauges one at each corner reinforcement bar. Fig. 11 shows the mean values of the strain time-history results for the concrete columns on the ground floor (P4_0, P5_0 and P8_0) and first floor (P4_1, P5_1, P7_1 and P8_1). The axial load in the central column (P5) at the ground and first floor remained fairly constant during the test.

After the sudden removal of P7 (loss of 150kN reaction), the load was redistributed dynamically to the nearby columns on the ground floor P4 (P4_0) and P8 (P8_0). The maximum shortening of columns P4 and P8 was 111.3$\mu\varepsilon$ (340kN) and 96.8$\mu\varepsilon$ (295kN) respectively, and their residual values were 67.2$\mu\varepsilon$ (205kN) and 57.0$\mu\varepsilon$ (174kN) respectively. The load increase in columns P4 and P8 was larger than the load of column P7 before the column removal (see Section 5.1). The maximum/residual ratio obtained was 1.7 for columns P4 and P8 which is representative of the dynamic amplification of the forces as discussed in Section 5.3.2. The maximum shortening of P4 and P8 during the push down step was 112.9$\mu\varepsilon$ (345kN) and 103.2$\mu\varepsilon$ (315kN) respectively.

The load redistribution on the first-floor columns was very different to that on the ground floor. The load in P7 in the first floor (P7_1) had a significant load reduction with a reduced mean deformation of 343.9$\mu\varepsilon$ (approximately 333kN – decompression) during the column removal step and 729.9$\mu\varepsilon$ (approximately 402kN – decompression) during the push down step. These results confirmed that column P7 at the first floor turn from compression to tension after the column removal. To calculate the load on the decompressed column P7 (P7_1) the cross sectional area was estimated using the homogenised section when the tensile stress was lower than the tensile strength (2.5MPa) whereas for larger tensile stresses only the reinforcement bars were considered. Regarding columns P4 and P8 at the first floor, the results in Fig. 11b show that the variations in the axial load were negligible, especially for the column removal step and for the beginning of the push down step where the deformations were low (less than 2mm).

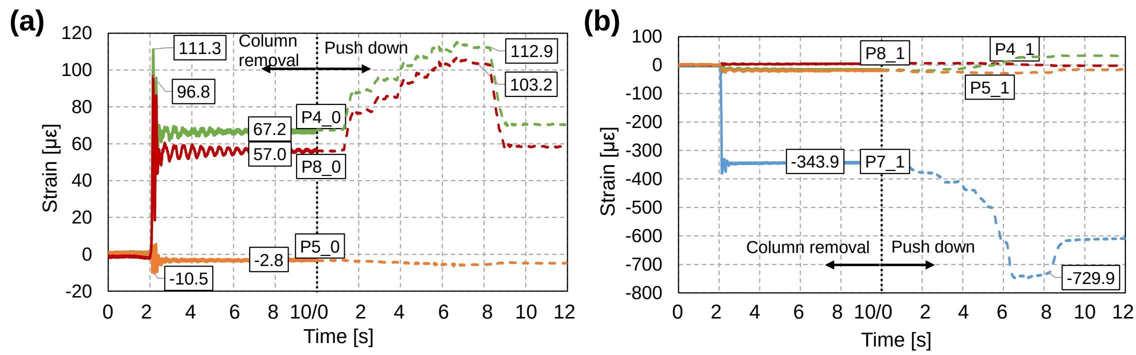

Fig. 11. Mean value of strain gauges on: (a) ground floor columns P4, P8 and P5; and (b) first floor columns P7, P4, P8 and P5. Positive values indicate shortening and negative decompression.

It can be concluded from these measurements that the infill masonry walls activated an ALP along their compressive diagonal as shown in Fig. 12. This was supported by the following evidence: a) the change in P7_1 from compression to tension; b) the negligible variations in load in columns P4 and P8 at the first floor; and c) the significant increase in compression in columns P4 and P8 at the ground floor. However, during the push down step and for deflections larger than 4mm (t=4s in the push down step, Fig. 5), the concrete structure started to work together with the infill walls and a transition towards Vierendeel action started to develop. This transition between two ALPs (at t=4s) was observed with increasing pulling load (Fig. 10) and deflections (Fig. 5) resulting in an increase of load in column P4_1 and a reduction in the variation of the tension load in column P7_1 as shown in Fig. 11b. The increase in the variation of the tension strains in P7_1 (Fig. 11b after t=4s) and the significant reduction of the resisting area (i.e. only reinforcement for large strains) resulted in an overall reduction in the variation of the tension load in the column.

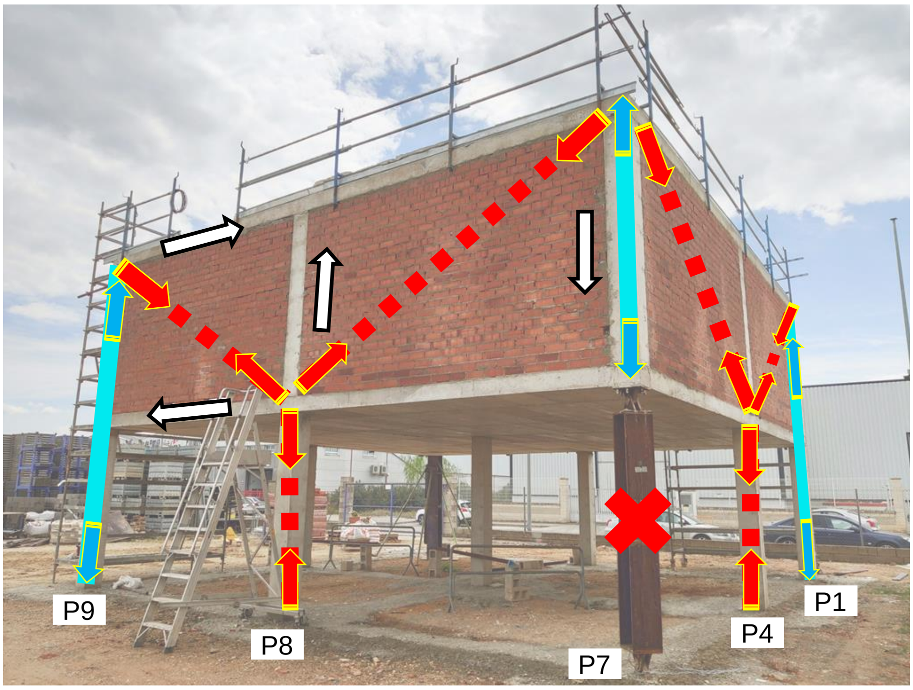

Fig. 12. Predominant load path of the structure after the sudden removal of column P7 and the later push down step (Note: white arrows denote shear distortion).

Further evidence of the transition from secondary truss to Vierendeel action was also evident from the large variations in the column bending moments at deflections larger than 4mm (achieved after 6s in the push down step shown in Fig. 13). Bending in the concrete frame was monitored from strain gauge readings on the columns. Fig. 13 shows an example of the strain readings in the ground floor (Fig.13a) and first floor (Fig. 13b) on P8.

In the column removal step, the strain gauges on P8 on the ground floor nearest to P7 (P8_04 and P8_02) had higher increased deformation (i.e. rotation of the slab-column joint towards P7). All the strain gauges on P8 on the ground floor showed variations in compressive deformation, confirming the predominance of axial over bending forces. However, this did not occur on the first floor, where there was a very small variation in the axial load and clear predominance of column bending towards the interior of the building (strain gauges P8_11 and P8_13 are in compression and strain gauges P8_12 and P8_14 in decompression).

In the push down step, the behaviour of ground floor column P8 was similar to that in the column removal step, although with significantly larger deformations. In the first floor, the axial load in P8 was constant but the moments in the outside (façade) frame increased significantly, as shown in Fig.13 (compressive strains in P8_11 and P8_12 and decompression strains in P8_13 and P8_14).

In summary, it can be concluded that the infill masonry walls had a strong influence in creating ALPs, with an even stronger influence in column removal step (secondary truss developed during the column removal phase) and a greater contribution of the concrete frame (transition towards Vierendeel action) in the push down step.

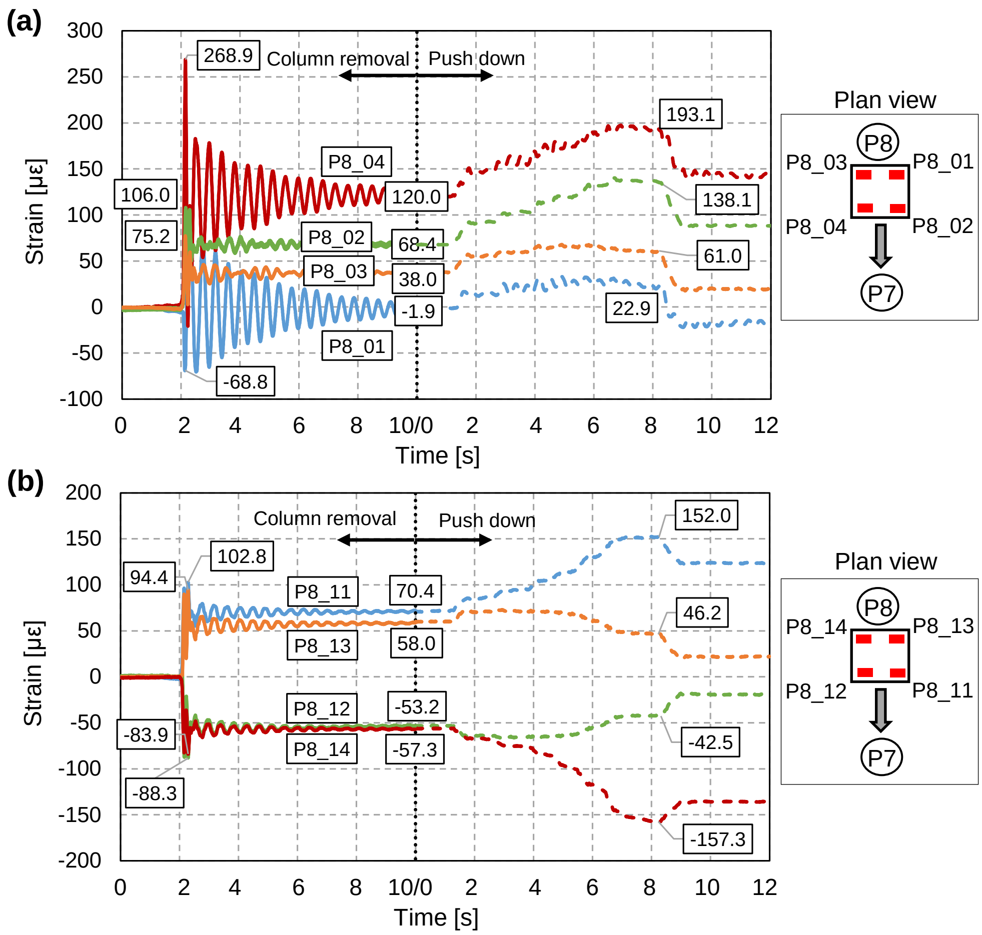

Fig. 13. Measures of strain gauges on ground (a) and first (b) floor column P8. The position of each strain gauge inside P8 is represented on the right of the figure. Positive values indicate shortening and negative decompression.

4.5. Acceleration

The vertical acceleration of the structure was recorded by an accelerometer at the bottom of P7 on the first floor (Fig. 14a) and the horizontal acceleration was measured at the top of P1 (Fig. 14b). The first vibrations were registered during the unlocking of the central hinge of the removed column and these were followed by others due to the sudden removal of the column. Vertical accelerations of up to 2.15g were measured, while the rebound reached 1.09g. Horizontal accelerations reached 0.32g towards P7 with a rebound of 0.50g.

The peak vertical acceleration in Fig. 14a was significantly larger than in the similar test without infill walls (Test 1 in Adam et al [26]) where a freefall type of motion was reported (accelerations near 1.0g). The higher peak accelerations obtained in Test 2 suggest the development of higher frequency modes of vibration near the removed column which in turn indicates that forces were transmitted through the column above.

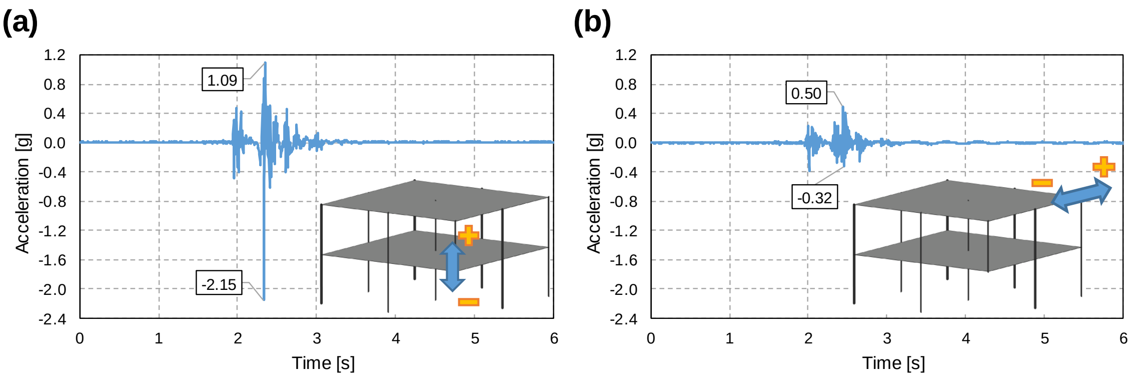

Fig. 14. Acceleration on columns P7 (a) and P1 (b); sensors Acc_P7_21V and Acc_P1_21H, respectively.

4.6. Residual damage after test

The concrete structure showed very little cracking; the only zone where some cracking was visible was on the bottom soffit of the second floor slab around P7. This column experienced large tensile stresses causing cracks in the column and in the connection with the second-floor slab (see Fig. 15a). Some detachment of the masonry-concrete interface took place at the column removal step which was more significant at the push down step as shown in Figs. 9 and 15. The crushing of some bricks was observed along the compressive diagonal after the push down step as shown in Fig. 15c. The damage observed on the structure was different from that experienced in a previous study without infill walls [26] which was due to bending and shear in the frame.

Fig. 15. Damage after the push down step: (a) top of column P7; (b) mortar-concrete interface on the top of column P4; and (c) crushed bricks due to compression forces near the top of column P7.

5. Analysis and discussion of the influence of infill walls on the response

This section analyses the influence of infill walls on structural behaviour after the sudden loss of a corner column by comparing the results from Test 2 presented in this paper with the results from identical Test 1 in Adam et al [26] without infill walls. The analysis of the results was divided into: a) load redistribution after column removal; b) ALPs; and c) LIFs/DAFs.

5.1. Load redistribution after column removal

The axial load in the column before it was removed was similar in Tests 1 and 2 as shown in Fig. 16. The load was estimated from the residual elongation measured in the steel column after the test. The axial load in the column before its removal was 140kN and 150kN for Test 1 and 2 respectively.

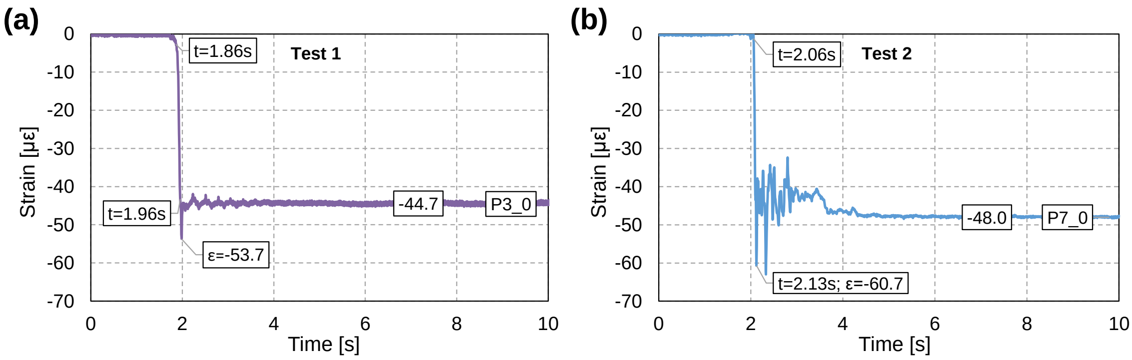

Fig. 16. Mean value of strain gauges of the ground floor steel columns P3 (test 1; Adam et al [26]**) and P7 (test 2). Negative values indicate decompression.**

After the P7 column removal in Test 2 (150kN), neighbouring columns P4 and P8 carried a significant increase in the axial load (load increment of 205kN and 174kN) due to moment transfer and the unloading of other columns (P1, P3 and P5). It is worth mentioning that in cases of internal column removal the neighbouring columns receive only a fraction of the load that was initially carried by the removed column [28]. For the neighbouring columns of this corner column removal test, the load redistribution was influenced by the lay-out of this specific building. Table 2 gives the residual mean deformation and axial force increments of P7, P4, P8, P1, P5 and P3 for the second test with infill masonry walls. All the ground-floor columns except P4 and P8 experienced a reduction of the axial loads (elongation). The experimental results obtained for the vertical reactions were consistent assuming that the load in column P9 reduced by a similar amount as P1 and that the reduction of the load in P2 and P6 was between the load reduction in P1 and P3. It was also observed that the load reduction in P1 was significantly larger than for P5 (closer to P7), which, together with the larger load increase in P4 and P8, underlines the importance of outside frames with infill masonry walls.

Table 2 gives the comparable results of the axial increments in the columns of Test 1 without infill walls from Adam et al. [26]. Although a similar load was removed, its redistribution was different, having around 60% higher positive axial force increments in closer columns (P4 and P8 in Test 2) and also higher negative axial force increments in other columns of the façade frame such as P1. This, together with the smaller axial load increments of other columns, implied that infill walls increased the influence of the façade frames on the load redistribution, and their columns will have greater compression or decompression when they include infill masonry walls.

Table 2. Analysis of the load redistribution after the sudden removal of column. Shortening strain increments are positive.

Test 1 (without infill walls)*			Test 2 (with infill masonry walls)		
Column	Residual mean strain [με]	Axial force increment [kN]	Column	Residual mean strain [με]	Axial force increment [kN]
P3 (removed)	-44.7	-140	P7 (removed)	-48.0	-150
P2	48.5	135	P4	67.2	205
P6	37.4	104	P8	57.0	174
P1	-8.9	-25	P1	-21.2	-64.7
P5	-7.6	-21	P5	-2.8	-9.3
P7	-3.6	-10	P3	-1.5	-4.7

*Values extracted from Adam et al [26].

5.2. Activation of Alternative Load Paths

As shown in Section 4.4 the infill masonry walls enabled the activation of the diagonal strut truss ALPs after the sudden corner-column removal and during part of the push down step (see Figs. 11-12). The results also showed that in order to activate the diagonal strut ALP, the load transfer relies on the development of a vertical tie through the column as shown in Fig. 12; first floor column P7_1 was in tension after column removal. This is relevant since in design the provision of vertical ties is not always feasible and the purpose of vertical ties has been questioned in the past on the basis that for tensile membrane action vertical ties are not needed. Test 2 also showed that towards the end of the push down step, when the deflections increased, a transition towards flexural and Vierendeel action was observed (see Section 4.4 for details). In Test 1 without infill masonry walls (Adam et al.[26]) it was shown that the predominant ALPs were Vierendeel and flexural actions. It can be concluded that infill walls in the façade frames can clearly modify the ALPs and this should be taken into account in designing building structures for the realistic representation of the structural behaviour in column removal scenarios.

Fig. 17 compares the vertical displacements in Tests 1 and 2; Fig. 17a shows the residual displacement profile along the first-floor slab towards the removed column. The results show that deformation in Test 2 (7.8mm) was significantly smaller than in Test 1 (48.1mm) due to the infill walls and therefore flexural and Vierendeel actions were more predominant in the later (i.e. columns experienced severe flexural deformations and slabs had a double curvature). Fig. 17b shows the horizontal displacement of P9 for Test 1 and Test 2 representing the drift of the structure. The lateral residual displacements were not uniform; in Test 1 it was approximately five times greater in the second floor than in the first floor whereas in Test 2 with infill walls the lateral displacement was negligible. In addition, lateral displacement in Test 2 was in the opposite direction in the first slab due to the effect of the masonry panels. After the column removal, the masonry panel above the removed column had a vertical distortion, activating a compressive diagonal (strut) between the first floor of P8 and the second floor of P7 (See arrows in Fig. 12). The resultant forces also activated a compressive diagonal (strut) between the first floor of P8 and the second floor of P9, producing a horizontal distortion of the infill panel (See arrows in Fig. 12). Finally, this behaviour was also confirmed by numerical simulations (See struts in Fig. 20).

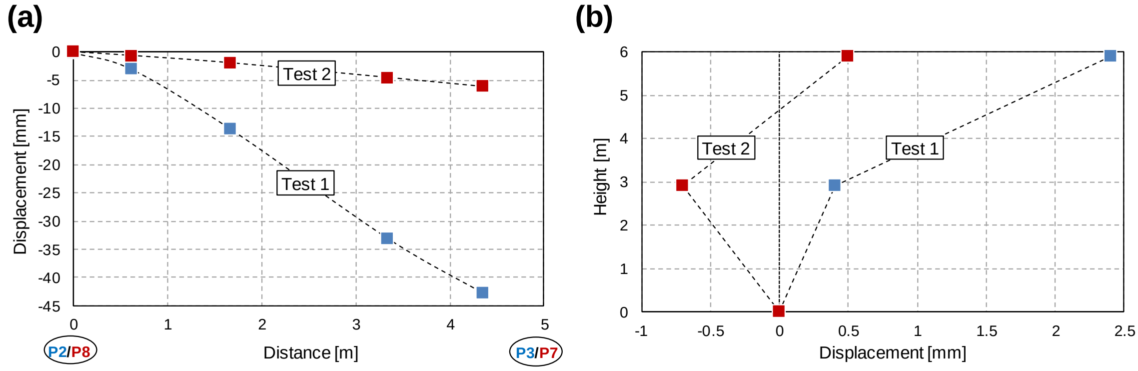

Fig. 17. (a) Vertical residual displacement (deformation) of the first floor between columns P2/P8 and P3/P7 for Test 1 and Test 2, respectively. (b) Horizontal residual displacement of column P9 for Test 1 and Test 2.

5.3. Load Increase Factors (LIFs) and Dynamic Amplification Factors (DAFs)

This section studies the influence of infill masonry walls on the Load Increase Factors (LIFs) and Dynamic Amplification Factors (DAFs), which are defined in international codes (e.g. GSA [3] or DoD [2]). LIFs and DAFs are used to facilitate the work of engineers and architects in designing structures for robustness using simplified analysis methods (e.g. linear static analyses) when considering advanced non-linear phenomena is impractical. Codes define DAFs in very general terms, and it has been shown in various studies [28–31] that they tend to over-estimate the structural forces and displacements after the sudden loss of a column.

In order to obtain LIFs and DAFs in this work, a linear (uncracked) static finite element analysis (LFEA) was carried out including the contribution of the infill walls. The use of LFEA is justified by some codes (DoD) for buildings without structural irregularities as well as irregular structures in which the estimated demand-capacity ratio from the linear analysis is less or equal than 2.0. The predicted stiffness of the masonry walls varied significantly depending on the masonry model adopted. A review of different alternative simplified models for infill masonry walls was carried out (see Section 5.3.1). Subsequently these models were applied in the LFEA and LIFs/DAFs were obtained and compared with those from a similar analysis carried in [26] for the same structure without infill walls (Section 5.3.2).

5.3.1. Masonry models adopted in the LFEA

Eight simplified macro-models were used to mimic the behaviour of the masonry infill wall in a reinforced concrete structure with the aim to replace the masonry assembly with a single equivalent elastic diagonal strut, acting only in compression, as shown in Fig. 18. Fig. 18 shows the geometrical parameters given by the building dimensions which were used to estimate the cross section of the equivalent strut (strut width w). To estimate the axial stiffness of the strut, the masonry’ secant modulus of elasticity (E_w) was estimated from empirical equations available in international standards (Table 3).

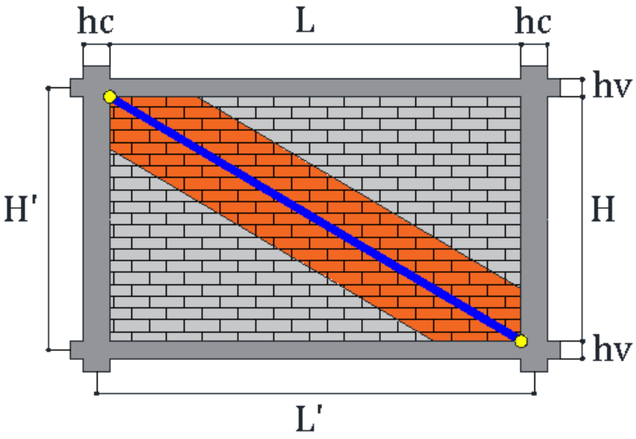

Fig. 18. Geometrical parameters employed in the current modelling approach.

As shown in Table 3, the secant modulus of elasticity of the masonry can be calculated from the characteristic compressive strength of the infill (f_k) which in turn depends on the compressive strength of the constituent materials. In the present work, the compressive strength of mortar (f_{mm}) and bricks (f_{bm}) was the average of the results of three compression tests given in Table 1. Eurocode 6 [32] was used to estimate the characteristic compressive strength of the masonry infill wall according to Eq. 1.

$$f_k = K \cdot f_{bm}^{0.7} \cdot f_{mm}^{0.3} \qquad [1]$$

where K is the coefficient of the type of block and mortar employed which was equal to 0.45 (value corresponding to 25%-55% hollow clay units, or Group 2 brick [32]). The characteristic compressive strength of the masonry f_k was equal to 6.97MPa. The secant modulus of elasticity was then calculated using Eq.2 given in Eurocode 6 [32].

$$E_w = K_E \cdot f_k \qquad [2]$$

where coefficient K_E was taken as 1000 in the absence of experimental data as recommended in [32]. Alternative values of K_E are shown in Table 3 using different international standards.

Table 3. Summary of K_E values proposed by different international standards and corresponding secant modulus of elasticity E_w obtained using Eq. 2

International Standard	K_E	E_w
Eurocode 6 [32]	1000	6976
ASCE/SEI, 2007 [33]	550	3837
Masonry Standards Joint Committee (MSJC), 1994 [34]	700	4883

Canadian Concrete Masonry Producers Association (CCMPA), 2009 [35]	850	5930
TEC: Turkish ministry of public works and settlements, 2007 [36]	200	1395

Geometrical parameters used to estimate the width of the equivalent strut are given in Table 4. The diagonal strut properties given in international standards can vary significantly. For example, Holmes [37] suggests that *w* should be taken as 33% of the diagonal length (*d*), while Paulay & Priestley [38] propose a value of 25% of *d*. Other parameters where differences were found include the contact between the adjacent column and the infill, the effective width of the strut w_e and the influence of the bending stiffness of the columns.

Table 4. Summary of the values adopted for geometrical parameters.

Symbol	Definition	Value	Units
L	Beam length	4700	[mm]
h_c	Column edge	300	[mm]
L’	Free span	5000	[mm]
H	Column height	2800	[mm]
h_v	Beam height	200	[mm]
H’	Free height	3000	[mm]
d	Equivalent strut length	5471	[mm]
θ	Angle formed by the equivalent strut	30.79	[°]
t_w	Thickness of the masonry infill	113	[mm]
E_c	Concrete elastic modulus of columns	28972	[MPa]
E_b	Concrete elastic modulus of beams	31654	[MPa]
I_c	Columns moment of inertia	6.75E8	[mm^4]
I_b	Beam moment of inertia	1.67E9	[mm^4]

Regarding the contact between the adjacent column and the infill, experimental studies showed that the bearing length is governed by the relative column-to-infill flexural stiffness. Its effect is considered in CCMPA [35] by introducing the vertical α_h and the horizontal α_L contact length (see Eqs. 3-4).

$$\alpha_h = \frac{\pi}{2}\sqrt[4]{\frac{4E_c I_c H}{E_w t_w \sin 2\theta}} \text{ (Vertical contact length)} \qquad [3]$$

$$\alpha_L = \pi\sqrt[4]{\frac{4E_b I_b L}{E_w t_w \sin 2\theta}} \text{ (Horizontal contact length)} \qquad [4]$$

The strut width *w* is given in Eq.5 and effective width w_e in Eq. 6.

$$w = \sqrt[2]{\alpha_h^2 + \alpha_L^2} \text{ (Width of the compressive strut)} \quad [5]$$

$$w_e = min \begin{cases} w/2 \\ d/4 \end{cases} \text{ (Effective width of the compressive strut)} \quad [6]$$

Regarding the effect of the bending stiffness of column and beams, Durrani et Luo [39] proposed a formulation for the strut width (Eqs. 7-9) similar to CCMPA [35].

$$m = 6\left(1 + \frac{6E_b I_b H\prime}{\pi E_c I_c L\prime}\right) \quad [7]$$

$$\gamma = 0.32\sqrt{sin\,2\theta}\left(\frac{H\prime^4 E_w t_w}{mE_c I_c H}\right)^{-0.1} \quad [8]$$

$$w = \gamma\, sin(2\theta)\, d \quad [9]$$

Conversely to [39], various standards propose simplified formulations taking into account only the column bending stiffness. Mainstone in 1971 [40] proposed calculating strut width by a modification of the equations in Smith & Carter in 1969 [41] where the equivalent strut width is given in Eq. 10-11-12.

$$\lambda = \sqrt[4]{\frac{E_w t_w \sin 2\theta}{4E_c I_c H}} \quad [10]$$

$$\lambda' = \lambda H' \quad [11]$$

$$w = 0.175\lambda_h^{-0.4} d \quad [12]$$

Different standards and research groups in the progressive collapse field adopt the equations described above, including ASCE/SEI, 2007 [33], TEC [36] and Qian and Li [20]. Alternative equations were proposed by Turgay et al. [42] and the Masonry Standards Joint Committee (MSJC) [34] as shown in Eq. 13-14 respectively.

$$w = 0.18\lambda_h^{-0.25} d \quad [13]$$

$$w = \frac{0.3}{\lambda \cos\theta} \quad [14]$$

Table 5 summarizes the models adopted in this work together with the values obtained of the secant modulus of the masonry infill and the strut width. Fig. 19 shows that the strut axial stiffness obtained varied significantly depending on the model used. The upper and lower estimates were obtained using Holmes [37] and TEC [36] formulae respectively. The TEC and MSJC recommendations provided unrealistically low estimates of the elastic modulus of the infill masonry walls; this was confirmed in subsequent LFEA described in Section 5.3.2.

Table 5. Summary of the formulation proposed by international standards and researchers.

International Standard and/or scholar	**Adopted E_w [MPa]**	**Strut width *w***	
		Proposed Eq.	**Value [mm]**
Eurocode 6	6976	---	---
ASCE/SEI, 2007	3837	$= 0.175\lambda_h^{-0.4}d$	584
Masonry Standards Joint Committee (MSJC), 1994	4883	$= \dfrac{0.3}{\lambda \cos\theta}$	286
Canadian Concrete Masonry Producers Association (CCMPA), 2009	5930	$min\begin{cases} w/2 \\ d/4 \end{cases}$	1368
TEC: Turkish ministry of public works and settlements, 2007	1395	$= 0.175\lambda_h^{-0.4}d$	646
Turgay et al., 2014	*CCMPA	$= 0.18\lambda_h^{-0.25}d$	703
Durrani et Luo, 1994	* Eurocode 6	$= \gamma \sin(2\theta)\, d$	981
Holmes, 1961	* Eurocode 6	= d/3	1824
Paulay & Priestley, 1992	* Eurocode 6	= d/4	1368

* adopted for the present study

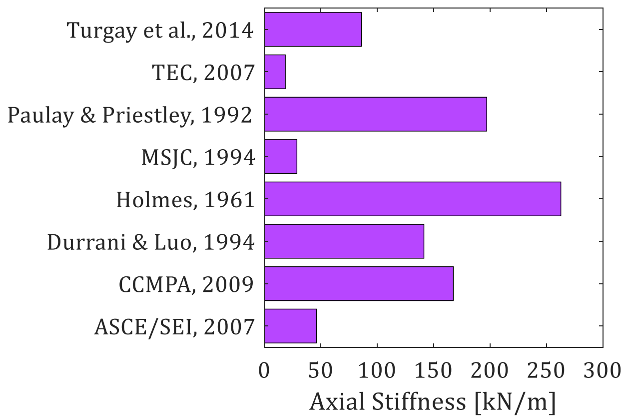

Fig. 19. Adopted axial stiffness of the diagonal strut to simulate the presence of infill masonry walls.

5.3.2. Influence of infill wall stiffness on LIFs and DAFs

The different values of the axial stiffness obtained in previous section (Fig. 19) were adopted in the LFEA to estimate the influence on LIFs and DAFs. Abaqus FE commercial software [43] was used, taking into account the concrete slabs, columns and masonry. The model comprised four-node shell elements for slabs and two-node beam elements for the columns, both having the same concrete linear mechanical properties (elastic modulus given in Table 1). The infill masonry walls were modelled using truss elements connecting opposite corners of the frame in the first floor and acting only in compression. Self-weight and live loads were applied in the model following the test arrangement. The linear static analysis was carried out, without any dynamic amplification factors introduced, using the building geometry after the column removal.

Fig. 20a shows the deformed RC building predicted after the corner column removal and Fig. 20b shows the vertical displacement at the point of the removed column obtained according to the different masonry models. Fig. 20b shows the vertical displacement measured in the test (red dashed lines) corresponding to the peak and residual displacements. In Test 2 the residual displacements can be assumed to be a good representation of the static displacements (i.e. displacements obtained if the column had been removed quasi-statically). This assumption is supported by the small deflections and negligible damaged observed in the structure after the column removal (Section 4.6); the same assumption is not applicable to Test 1 without infill walls (Adam et al.[26]). Fig. 20b shows that the LFEA with models from ASCE/SEI 2007 [33] and Turgay et al. [42] provided the most realistic predictions whereas models TEC [36] and MSJC [34] provided incorrect answers (i.e. vertical displacement from a linear-static analysis should be less than the peak test value). The latter two models clearly underestimate the masonry infill wall stiffness after column removal and therefore they were not used in subsequent calculations. The variations in the axial stiffness in the remaining six models and resulting displacements could potentially be addressed by giving different recommended values of DAFs for each model.

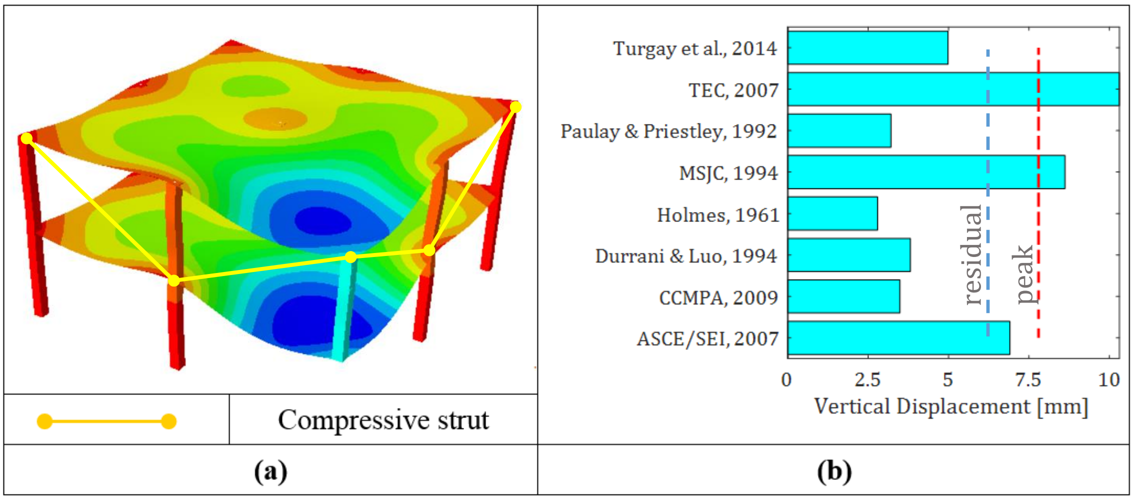

Fig. 20. Numerical model (a) and comparison of experimental (dashed lines) and numerical vertical displacements of compressive struts (b).

Table 6 gives the amplification factors obtained for the vertical displacement DAF_{LD} defined as the ratio between the dynamic value obtained experimentally (peak) and the static value from the LFEA; this is also defined in DoD [2] as Load Increase Factor LIF. The values obtained of DAF_{LD} ranged from 1.13 to 2.79 (lower values correspond to results using lower stiffness of the infill walls). Values of DAF_{LD} lower than 2.0 seems to contradict DoD [2] recommendations, where for two-way slabs and slab-column connections DAF_{LD} can vary between 2.0 and 3.2 depending on the ductility of the connections. However, these recommendations are based on numerical results from bare frame analyses where the additional stiffness and damping from the infill walls was neglected. DAF_{LD} lower than 2.0 could be justified in cases where the mechanical non-linear component of DAF is negligible and the dynamic component is estimated from testing. The dynamic amplification of the displacements based on the test results only (assuming that the residual displacement is representative of the static value) was around 1.25 (Section 4.1) which was justified on damping and some small mechanical non-linearities (damage). It is known that infill walls on bare frames introduce a source of structural damping [44]. For this test with masonry infill walls, the maximum experimental damping factor obtained was 21% whereas for Test 1 without infill walls the damping ratio was 6%. Considering a linear single degree of freedom system with 21% damping DAF would be 1.5 [45]. Further research is needed to investigate the influence of the main masonry properties and openings on the strut stiffness and damping introduced in the building since this can have a significant influence on the recommended value for DAF_{LD}. It is also worth noting that for irregular geometries and loading situations significantly different to the case studied a proper nonlinear dynamic analysis will be required instead of using simplified values of DAF_{LD}.

Table 6. Estimated DAF_{LD} with the proposed models.

Model	ASCE/SEI, 2007	CCMPA, 2009	Durrani et Luo, 1994	Holmes, 1961	Paulay& Priestley, 1992	Turgay et al., 2014
DAF_{LD}	1.13	2.23	2.04	2.79	2.43	1.56

Regarding the dynamic amplification of forces, DoD [2] recommends using a different factor (DAF_{LF}) with a fixed value of 2.0. The total experimental axial force in columns P4 and P8 was estimated as the initial force in the column (232kN from a linear FE analysis) plus the peak axial force increment obtained in the test after the column removal. Table 7 shows the axial force increments obtained experimentally and numerically (LFEA). The DAF_{LF} shown in Table 7 was obtained using the average of the total experimental axial force between P4 and P8 (232+(340+295)/2 = 550kN) and the sum of 232kN to the axial force increment obtained for each diagonal strut model (e.g. 550/(232+118) = 1.57 for the ASCE/SEI 2007 strut model). DAF_{LF} ranged from 1.48 to 1.57, which is a relatively narrow range, showing that diagonal strut stiffness had no significant effect on DAF_{LF}. The maximum value of DAF_{LF} (1.57) was clearly below the recommended (2.0) by DoD [2]. This was also consistent with the dynamic amplification obtained directly from the test, which was around 1.65-1.70 (Section 4.4), assuming that the residual axial loads are representative of the static values (see also comments on damping in the previous paragraph).

It can be concluded that the proposed DAF_{LD} and DAF_{LF} values in Table 6 and Table 7 could be used as LIF and DAFs respectively (following the definition of DoD [2]) in alternative load path calculations by means of a simple LFEA to consider in a relatively simpler manner the combined effect of nonlinear and inertial effects.

Table 7. Estimated DAF_{LF} with the proposed models.

Axial force increments [kN]							
Experimental		Different diagonal strut models					
Column P4	Column P8	ASCE/SEI, 2007	CCMPA, 2009	Durrani et Luo, 1994	Holmes, 1961	Paulay & Priestley, 1992	Turgay et al., 2014
340	295	118	133	130	139	135	124
DAF_{LF} (based on total axial forces)		1.57	1.51	1.52	1.48	1.50	1.54

Table 8 shows the comparison of the DAFs obtained in Test 1 without infill walls (Adam et al. [26]) and Test 2 with infill masonry walls. An increase of the DAF_{LF} was observed of around 20% due to the presence of the infill masonry walls. This interesting finding can be justified on the increase of load transferred to the adjacent columns due to the diagonal strut; the residual axial load in Test 2 was 60% larger than in Test 1. In a nonlinear system, the additional kinematic energy introduced by increasing the load applied suddenly, results in a larger amplification of the load as shown in Sagaseta et al. [29]. The results show that the DAF_{LF} is not highly influenced by the masonry properties nor the model adopted for the diagonal strut but the same is not true for the displacements DAF_{LD}. The factors for deflections can be above 2.0 for cases with or without infill walls when the linear-static model used to estimate the deflections gives lower estimates (i.e. a LFEA in Test 1 or a LFEA with masonry models with relatively high stiffness). For DAF_{LD} one could adopt a conservative value of 2.7 for cases with and without infill walls or more refined values varying on the masonry assembly properties or new ones if further test become available for other types of infill walls.

Table 8. DAF comparison between Test 1 without infill walls and Test 2 with infill masonry walls.

	DAF_{LD}	DAF_{LF}
Test 1 (Adam et al. [26])	2.64	1.24
Test 2	[1.13-2.79]	[1.48-1.57]

6. Conclusions

This study analyses the influence of infill masonry walls in buildings subjected to the sudden removal of a corner-column. The results from a purpose-built full-scale RC building structure with masonry infill walls are presented in this paper and compared to the results from a similar test without infill walls published by the authors [26]. The test presented herein included a sudden column removal step followed by a push down step. From the results obtained the following conclusions can be drawn:

- The two tests compared in this work (with and without infill panels) had a similar load in the corner column prior to the removal of the column (140kN and 150kN without and with infill walls respectively). After the column removal, significant changes were observed between both tests in terms of alternative load paths, deflections and dynamic amplifications.
- The results from the test with infill walls confirmed their strong influence on the activation of different ALPs especially in the column removal phase leading to very small deflections compared to cases without infill walls. The response was governed by the activation of diagonal struts which relied heavily on the vertical tie through the column. In general, vertical tying would be significant mainly in the immediate floor above the removed column in a multi-storey building. This is relevant as vertical ties are not always considered in design.
- The infill walls increased the influence of the façade frames on the load redistribution with a significant increase of the axial loads transmitted to the adjacent column (P4 and P8) to the removed column. In the test with infill wall the increase in axial loads in the adjacent columns was 60% larger than in the test without infill walls.
- In the push down step, as deformations increased, a larger contribution of the concrete structure was observed. This response demonstrated the transition to flexural and Vierendeel effect which was predominant in the test without infill walls.

- Different masonry macro-models can be used to estimate the diagonal stiffness of the infill walls although some models can provide unrealistically low predictions. These models can be adopted in linear-static analyses in combination with appropriate dynamic amplification factors which are provided in this work for regular buildings.
- It was found that the dynamic amplification factor of the load increased from 1.24 to around 1.50 due to the infill walls. This was due to the additional sudden load transferred to adjacent columns through the diagonal struts. The dynamic amplification of the load was not highly influenced by the properties of the masonry whereas the same was not true for the amplification of the deflections. A value of DAF_{LD} of around 2.7 could be applied to LFEA without and with infill walls, although this might be overly conservative for cases with infill walls in which the stiffness of the masonry is estimated accurately or slightly underestimated..

Further research is needed to investigate the influence of masonry properties and openings on the strut stiffness and damping introduced in the building; they may be highly dependent on the proposed DAF_{LD}. For irregular geometries and loading scenarios significantly different to the case studied, an extensive parametric study (with a proper nonlinear dynamic analysis) will be required before determining appropriate ranges for DAF_{LF} and DAF_{LD}.

Acknowledgements

This work was carried out with the support of a 2017 Leonardo Grant for Researchers and Cultural Creators from the BBVA Foundation. The authors would also like to express their gratitude to the *Levantina, Ingeniería y Construcción S.L.* (LIC) company for funding the construction of the building, and to the *Generalitat Valenciana*/*Fons Social Europeu* [APOSTD/2019/101] and *Universitat Politècnica de València* [PAID-10-17] for funding received under different postdoctoral programs.

References

[1] American Society of Civil Engineers (ASCE). Minimum Design Loads for Buildings and Other Structures (ASCE/SEI 7-05). Struct Eng Inst ASCE 2005.

[2] DoD. Department of Defense. Design of buildings to resist progressive collapse (UFC 4-023-03); 2009.

[3] GSA. General Services Administration. Progressive collapse analysis and design guidelines for new federal office buildings and major organization projects; 2013.

[4] EN 1991-1-7. Eurocode 1: Actions on structures - Part 1-7: General actions - Accidental actions; 2006.

[5] Adam JM, Parisi F, Sagaseta J, Lu X. Research and practice on progressive collapse and robustness of building structures in the 21st century. Eng Struct 2018;173:122–49. doi:10.1016/j.engstruct.2018.06.082.

[6] Ellingwood BR, Smilowitz R, Dusenberry DO, Duthinh D, Lew HS, Carino NJ. Best practices for reducing the potential for progressive collapse in buildings. US Natl Inst Stand Technol (NIST) Dep Commer 2007:216.

[7] Baker JF, Williams EL, Lax D. The Design of Framed Buildings against High-Explosive Bombs. Civ. Eng. war - Inst. Civ. Eng., London: Thomas Telford Ltd; 1948, p. 80–112. doi:10.1680/ciwv3.45170.0006.

[8] Christopherson DG. Structural Defence. London: Ministry of Home Security Research & Experiments Department; 1945.

[9] Miller D, Doh J-H. Peak factors of non-gaussianwind force. Struct Des Tall Spec Build 2012;24:421–39. doi:10.1002/tal.

[10] Kim J, Lee H. Progressive collapse-resisting capacity of framed structures with infill steel panels. J Constr Steel Res 2013;89:145–52. doi:10.1016/j.jcsr.2013.07.004.

[11] Xavier FB, Macorini L, Izzuddin BA, Chisari C, Gattesco N, Noe S, et al. Pushdown Tests on Masonry Infilled Frames for Assessment of Building Robustness. J Struct Eng 2017;143:1–13. doi:10.1061/(ASCE)ST.1943-541X.0001777.

[12] Eren N, Brunesi E, Nascimbene R. Influence of masonry infills on the progressive collapse resistance of reinforced concrete framed buildings. Eng Struct 2019;178:375–94. doi:10.1016/j.engstruct.2018.10.056.

[13] Yu J, Gan YP, Wu J, Wu H. Effect of concrete masonry infill walls on progressive collapse performance of reinforced concrete infilled frames. Eng Struct 2019;191:179–93. doi:10.1016/j.engstruct.2019.04.048.

[14] Hafez I, Khalil A, Mourad S. Alternate path method analysis of RC structures using applied element method. Int J Prot Struct 2013;4:45–64. doi:10.1260/2041-4196.4.1.45.

[15] Farazman S, Izzuddin BA, Cormie D. Influence of Unreinforced Masonry Infill Panels on the Robustness of Multistory Buildings. J Perform Constr Facil 2013;27:673–82. doi:10.1061/(ASCE)CF.1943-5509.0000392.

[16] Helmy H, Hadhoud H, Mourad S. Infilled masonry walls contribution in mitigating progressive collapse of multistory reinforced concrete structures according to UFC guidelines. Int J Adv Struct Eng 2015;7:233–47. doi:10.1007/s40091-015-0094-5.

[17] Xavier FB, MacOrini L, Izzuddin BA. Robustness of multistory buildings with masonry infill. J Perform Constr Facil 2015;29:1–12. doi:10.1061/(ASCE)CF.1943-5509.0000684.

[18] Shan S, Li S, Xu S, Xie L. Experimental study on the progressive collapse performance

of RC frames with infill walls. Eng Struct 2016;111:80–92. doi:10.1016/j.engstruct.2015.12.010.

[19] Li S, Shan S, Zhai C, Xie L. Experimental and numerical study on progressive collapse process of RC frames with full-height infill walls. Eng Fail Anal 2016;59:57–68. doi:10.1016/j.engfailanal.2015.11.020.

[20] Qian K, Li B. Effects of Masonry Infill Wall on the Performance of RC Frames to Resist Progressive Collapse. J Struct Eng 2017;143:1DUMMY. doi:10.1061/(ASCE)ST.1943-541X.0001860.

[21] Brodsky A, Yankelevsky DZ. Resistance of reinforced concrete frames with masonry infill walls to in-plane gravity loading due to loss of a supporting column. Eng Struct 2017;140:134–50. doi:10.1016/j.engstruct.2017.02.061.

[22] Baghi H, Oliveira A, Valença J, Cavaco E, Neves L, Júlio E. Behavior of reinforced concrete frame with masonry infill wall subjected to vertical load. Eng Struct 2018;171:476–87. doi:10.1016/j.engstruct.2018.06.001.

[23] Brodsky A, Yankelevsky DZ. Resistance of reinforced concrete frames with masonry infill walls to in-plane gravity loading due to loss of a supporting column. Eng Struct 2017;140:134–50. doi:10.1016/j.engstruct.2017.02.061.

[24] Brodsky A, Rabinovitch O, Yankelevsky DZ. Determination of the interaction between a masonry wall and a confining frame. Eng Struct 2018;167:214–26. doi:10.1016/j.engstruct.2018.04.001.

[25] Ma F, Gilbert BP, Guan H, Xue H, Lu X, Li Y. Experimental study on the progressive collapse behaviour of RC flat plate substructures subjected to corner column removal scenarios. Eng Struct 2019;180:728–41. doi:10.1016/j.engstruct.2018.11.043.

[26] Adam JM, Buitrago M, Bertolesi E, Sagaseta J, Moragues JJ. Dynamic performance of a real-scale reinforced concrete building test under corner-column failure scenario. Eng Struct 2020;210:110414.

[27] EN 1990. Eurocode: Basis of structural design; 2002.

[28] Olmati P, Sagaseta J, Cormie D, Jones AEK. Simplified reliability analysis of punching in reinforced concrete flat slab buildings under accidental actions. Eng Struct 2017;130:83–98. doi:10.1016/j.engstruct.2016.09.061.

[29] Sagaseta J, Ulaeto N, Russell J. Structural robustness of concrete flat slab structures. ACI Struct J 2017;315:273–98.

[30] Qian K, Li B. Experimental study of drop panel effects on response of reinforced concrete flat slabs after loss of corner column. ACI Struct J 2013:845–56.

[31] Russell JM, Owen JS, Hajirasouliha I. Experimental investigation on the dynamic response of RC flat slabs after a sudden column loss. Eng Struct 2015;99:28–41. doi:10.1016/j.engstruct.2015.04.040.

[32] EN 1996-1-1: Eurocode 6: Design of masonry structures - Part 1-1: General rules for reinforced and unreinforced masonry structures. 2005.

[33] ASCE/SEI. Standard 41-06: Seismic Rehabilitation of Existing Structures. ASCE 2007. Reston, Virginia, USA 2007.

[34] Masonry Standards Joint Committee (MSJC). Builiding code requirements and specification for masonry structures and related commentaries. American Concrete Institute, Farmington Hills 1994.

[35] Anderson D, Brzev S. Seismic design fuide for masonry buildings - Canadian Concrete

Masonry Producers Association. 2009.

[36] The ministry of public works and settlements. Turkish Code for Buildings in Seismic Zones (TEC). Ankara, Turquía 2007.

[37] Holmes M. Steel frames with brickwork and concrete infilling. ICE Proc, 1961;19:473–8.

[38] Paulay, T. & Pristley MJN. Seismic design of reinforced concrete and masonry buildings,. New York A Wiley Intersci Publ 1992.

[39] Durrani A.J. & Luo Y.H. Seismic retrofit of flat-slab buildings with masonry infills. Buffalo, New York Natl Cent Earthq Eng Res (NCEER) 1994.

[40] Mainstone R.J. On the stiffness and strengths of infilled frames. ICE Suppl., 1971;4.

[41] Smith B.S. & Carter C. A method of analysis for infilled frames. ICE Proc, 1969;44:31–48.

[42] Turgay T., Durmus M.C., Binici B. & Ozcebe G. Evaluation of the Predictive Models for Stiffness, Strength, and Deformation Capacity of RC Frames with Masonry Infill Walls. J Struct Eng 2014:1–9.

[43] Abaqus. Release 6.14. Theory and user’s manuals. Pawtucket (RI, USA): Hibbit, Karlsson and Sorensen Inc.. 2014.

[44] Ozkaynak H, Yuksel E, Yalcin C, Dindar AA, Buyukozturk O. Masonry infill walls in reinforced concrete frames as a source of structural damping. Earthq Eng Struct Dyn 2014;43:949–68. doi:10.1002/eqe.2380.

[45] Biggs JM. Introduction to Structural Dynamics. New York; San Francisco; Toronto; London: McGraw-Hill, Inc; 1964.